

**General relativistic  $N$ -body simulations in the weak field limit**Julian Adamek,<sup>1,\*</sup> David Daverio,<sup>1,†</sup> Ruth Durrer,<sup>1,‡</sup> and Martin Kunz<sup>1,2,§</sup><sup>1</sup>*Département de Physique Théorique & Center for Astroparticle Physics,**Université de Genève, Quai E. Ansermet 24, CH-1211 Genève 4, Switzerland*<sup>2</sup>*African Institute for Mathematical Sciences, 6 Melrose Road, Muizenberg, 7945, South Africa*

(Received 30 August 2013; published 22 November 2013)

We develop a formalism for general relativistic  $N$ -body simulations in the weak field regime, suitable for cosmological applications. The problem is kept tractable by retaining the metric perturbations to first order, the first derivatives to second order, and second derivatives to all orders, thus taking into account the most important nonlinear effects of Einstein gravity. It is also expected that any significant “back-reaction” should appear at this order. We show that the simulation scheme is feasible in practice by implementing it for a plane-symmetric situation and running two test cases, one with only cold dark matter, and one which also includes a cosmological constant. For these plane-symmetric situations, the deviations from the usual Newtonian  $N$ -body simulations remain small and, apart from a nontrivial correction to the background, can be accurately estimated within the Newtonian framework. The correction to the background scale factor, which is a genuine backreaction effect, can be robustly obtained with our algorithm. Our numerical approach is also naturally suited for the inclusion of extra relativistic fields and thus for dark energy or modified gravity simulations.

DOI: [10.1103/PhysRevD.88.103527](https://doi.org/10.1103/PhysRevD.88.103527)

PACS numbers: 98.80.-k, 04.25.D-, 04.25.Nx, 95.30.Sf

**I. INTRODUCTION**

Cosmological late-time calculations and simulations are usually divided into two distinct approaches, linear perturbation theory of general relativity (GR) and Newtonian  $N$ -body simulations. Linear perturbation theory is used on large scales where perturbations are small, so that higher-order terms can safely be neglected. On small scales on the other hand, Newtonian gravity provides a very good approximation to the dynamics of nonrelativistic massive particles.

This distinction however breaks down in at least two, and maybe three, cases.

The first case concerns the addition of relativistic fields in a context where nonlinearities are important. An example is the impact of topological defects on the formation of structure [1] or the effect of modified-gravity (MG) theories on gravitational clustering on small scales, see [2] and references therein. In this case we have to simulate the nonlinear dynamics at least for the matter perturbations, and in general also for the fields, as MG theories generically need nonlinear screening mechanisms that become important on small scales. Newtonian gravity is usually not appropriate as e.g. both topological defects [3,4] and MG theories [5] exhibit a nontrivial anisotropic stress that leads to a gravitational slip which cannot be included in standard  $N$ -body simulations.

The second case is due to the ongoing revolution in observational cosmology where surveys are now reaching

unprecedented sizes, mapping out a significant fraction of the observable Universe. On large scales and at large distances it becomes necessary to take into account relativistic effects [6–11]. Although small, the impact of the perturbations, e.g., on distance measurements, is not negligible and can either be used as an additional probe of cosmology (e.g. [12,13]) or lead to an additional noise in the measurements [14,15] that may already be relevant for e.g. the Planck satellite results [16,17]. A general relativistic extension of  $N$ -body simulations will automatically include these effects, and since the metric is fully known, this will in addition allow us to integrate the geodesic equation of photons through the simulation volume to obtain accurate predictions for observations that include all relevant relativistic effects.

If we implement a numerical scheme that is able to follow the relativistic evolution of the Universe, we are then also able to test the third (and more speculative) case for a general relativistic framework for cosmological simulations in the nonlinear regime: GR is a nonlinear theory, and in principle nonlinear effects on small scales can “leak” to larger scales and lead to unexpected nonperturbative behavior. This idea is often called “backreaction” (see e.g. [18–22] for some recent reviews). If it is realized in nature, it would link the recent onset of accelerated expansion to the beginning of nonlinear structure formation and so provide a natural solution to the coincidence problem of dark energy. This cannot easily be checked within Newtonian simulations as the terms from backreaction e.g. in the Buchert formalism [19] become total derivatives in the Newtonian approximation and therefore do not contribute in a simulation with periodic boundary conditions [23].

\*julian.adamek@unige.ch

†david.daverio@unige.ch

‡ruth.durrer@unige.ch

§martin.kunz@unige.ch

However, it is very difficult to test backreaction analytically due to the nonlinear nature of the problem, and a numerical GR simulation appears to be the most straightforward way to rigorously test this possibility. This test of backreaction is in a sense a bonus on top of the important applications of such a code for precision cosmology in general and especially in the dark sector.

While it would be desirable to simulate cosmology in a fully general relativistic way, this is technically very challenging, as demonstrated by the efforts necessary to simulate, for example, black hole mergers over just a short period of time; see [24] and references therein. We therefore need a scheme that captures the features of general relativity that are relevant for cosmology, without the overhead of using full GR. This can be done by first assuming that, as in linear perturbation theory, our Universe on very large scales is close to being isotropic and homogeneous, i.e., has a metric close to the Friedmann-Lemaître-Robertson-Walker (FLRW) class and can thus be taken to have a line element (keeping for the moment only the scalar perturbations, and assuming a flat FLRW background universe) of the form

$$ds^2 = a^2(\tau)[-(1 + 2\Psi)d\tau^2 + (1 - 2\Phi)d\mathbf{x}^2]. \quad (1)$$

The success of linear perturbation theory for the analysis of perturbations in the cosmic microwave background (CMB) indicates that the gravitational potentials as well as perturbations in the matter distribution like  $\delta \doteq \delta\rho/\bar{\rho}$  are small on large scales. However, the existence of galaxies, suns, planets, and cosmological observers requires that at least the matter perturbations become large on small scales, with  $\delta \gg 1$ . On small scales we expect that the matter perturbations and the gravitational potential are connected to a high accuracy by Poisson's equation,

$$\Delta\Phi = 4\pi G a^2 \bar{\rho} \delta. \quad (2)$$

In Fourier space  $\Delta\Phi$  becomes  $-k^2\Phi$ , and on small scales the wave number  $k$  is large, so that  $\delta$  can become large even if the potential  $\Phi$  remains small on *all* scales. Indeed, the potential is expected to remain small since it is small initially and it does not grow within linear perturbation theory.

The approach that we adopt is then to keep the gravitational potentials always only to first order, but to be more careful with spatial derivatives. We keep first derivatives of  $\Phi$  and  $\Psi$  (and therefore also velocities) to second order, and second and higher spatial derivatives of the potentials (and therefore also  $\delta$ ) to all orders. The theoretical foundations of this approach have been laid out recently in [25,26]. Here, we want to take it an important step further and develop the technology for its numerical application. See also [27,28] for a study of relativistic corrections to particle motion.

Notice that this weak field limit is enough to at least *test* for strong backreaction effects: as long as the metric perturbations remain small, we know that we are within the domain of validity of our approximations. If however they

become large, then our scheme breaks down, but we learn in this case that the standard approaches to cosmological predictions break down as well. This enables us to diagnose the failure in our approach, and to recognize whether we need to go beyond the weak-field limit.

In this paper we mainly describe our formalism and the numerical algorithms, and perform tests in a plane symmetric situation. The application to realistic cosmological models in three spatial dimensions and a detailed comparison with Newtonian  $N$ -body simulations will be presented in a forthcoming paper. An application to observations in plane symmetric universes and a comparison with exact relativistic solutions is discussed in an accompanying paper [29].

The outline of this paper is as follows: in the next section we describe our approximation scheme and present the basic equations. In Sec. III we outline the numerical implementation. In Sec. IV we apply it to a simple, plane-symmetric case. We discuss the results and conclude in Sec. V. Some details of the numerical implementation and the generation of initial data are deferred to two Appendices.

## II. APPROXIMATION SCHEME AND FUNDAMENTAL EQUATIONS

When we go beyond linear perturbations, the line element (1) does not allow for a self-consistent description of cosmology, as scalar, vector, and tensor perturbations start to mix. We therefore use in this paper the more general line element which admits also vector and tensor modes,

$$ds^2 = a^2(\tau)[-(1 + 2\Psi)d\tau^2 - 2B_i dx^i d\tau + (1 - 2\Phi)\delta_{ij} dx^i dx^j + h_{ij} dx^i dx^j]. \quad (3)$$

In order to remove the gauge freedom we restrict  $B_i$  to be a pure vector mode and  $h_{ij}$  to be a pure tensor perturbation. To this end we choose the transverse/traceless gauge conditions  $\delta^{ij}B_{i,j} = \delta^{ik}h_{ij,k} = \delta^{ij}h_{ij} = 0$ , as was done in [26]. The above line element and gauge conditions can be imposed without loss of generality, i.e. we are not restricting the class of solutions, as long as we are interested in solutions which are not too far away from FLRW and hence have a cosmological interpretation. On the other hand, even if the perturbations become large, e.g.  $|\Psi| \gtrsim 1$ , it is not clear that deviations from the Friedmann background are significant. It might just be that the longitudinal gauge becomes badly adapted. This has been observed in some models of the early Universe, see e.g. [30,31], but is not expected to occur in a situation which is close to Newtonian gravity.

Having abandoned the Newtonian concept of absolute space, index placement has become meaningful and must be treated accordingly. For convenience, and to avoid ambiguity or confusion, we will always consider the perturbations  $B_i$  and  $h_{ij}$  with covariant indices only, and explicitly write the Euclidean metric wherever it is needed for index contraction. We use the notation  $f_{,i} \doteq \partial f / \partial x^i$ ,

$\Delta f \doteq \delta^{ij} \partial^2 f / \partial x^i \partial x^j$ , and a prime  $'$  to denote  $\partial / \partial \tau$ . Latin indices take values 1, 2, 3, while Greek indices run from 0 to 3, and a sum is implied over repeated indices.

Except for very particular, symmetric cases, solving Einstein's equations can only be achieved in approximation. The approximation scheme we use here is well adapted for cosmological settings where one is interested in the solution far away from compact sources (like black holes) and one can therefore consider a weak field limit. However, we clearly want to go beyond linear perturbation theory in order to allow for matter perturbations to evolve fully into the nonlinear regime of structure formation. We will therefore use an approach that is equivalent to the formalism of [25,26] who have adapted a shortwave approximation in order to treat small scale inhomogeneities in cosmology. In this approach it is assumed that large (nonlinear) matter perturbations generally occur on small spatial scales, an assumption that is well supported by observations. Accordingly, spatial derivatives of metric perturbations should have a larger weight in a perturbative expansion than the metric perturbations themselves. In fact, gravitational potentials are of the order of  $\sim 10^{-5}$  from galactic scales out to the scales of CMB observations. Gradients, on the other hand, need not be that small. They are related to peculiar velocities, and these are typically observed to be of the order of  $\sim 10^{-3}$  on galactic and cluster scales, see [32] and references therein. Second spatial derivatives are related to the density contrast, which becomes nonperturbative, i.e. larger than unity.

In more detail, the approximation scheme<sup>1</sup> we want to implement amounts to giving every spatial derivative a weight  $\epsilon^{-1/2}$  where  $\epsilon$  is a weight characterizing the smallness of the metric perturbations. We then consistently keep

all the terms up to order  $\epsilon$ . This means that we keep terms which are linear in the metric perturbations either by themselves or multiplied with second spatial derivatives which are considered to be of  $\mathcal{O}(1)$ , so that we are accurate to  $\mathcal{O}(\epsilon)$ . In addition, we retain quadratic terms of first spatial derivatives. As velocities are expected to be of the same order as gradients, we go to quadratic order also here to remain self-consistent. Correspondingly, we have to keep density fluctuations, which are of  $\mathcal{O}(1)$  multiplied with metric perturbations or with squared velocities and squared spatial derivatives of metric perturbations. Time derivatives are simply given the same weight as the quantity they act upon. This means, however, that we do not take a quasistatic limit where time derivatives are neglected altogether.

On very large scales, where all perturbations remain small, the scheme is equivalent to relativistic linear perturbation theory since we do not, for instance, keep terms which are quadratic in the metric perturbations themselves. On these scales, linear perturbation theory is very accurate because second-order corrections are expected to be of the order of  $\sim 10^{-10}$ . On intermediate and small scales, however, the scheme takes into account also the most important nonlinear relativistic terms. Since we stay in a relativistic framework throughout, we ensure that gauge issues are automatically addressed in the correct way such that we could easily construct all kinds of gauge invariant observables consistently. Such observables are, however, not the focus of this paper, which is aimed at the development of the necessary tools.

With the metric (3) and our choice of gauge, the components of the Einstein tensor read

$$G_0^0 + 3 \frac{\mathcal{H}^2}{a^2} = \frac{2}{a^2} \left[ 3\mathcal{H}\Phi' + 3\mathcal{H}^2\Psi - (1 + 4\Phi)\Delta\Phi - \frac{3}{2}\delta^{ij}\Phi_{,i}\Phi_{,j} \right], \quad (4a)$$

$$G_i^0 = -\frac{2}{a^2} \left[ \frac{1}{4}\Delta B_i + \Phi'_{,i} + \mathcal{H}\Psi_{,i} \right], \quad (4b)$$

$$\begin{aligned} G_j^i + \delta_j^i \left( 2\frac{\mathcal{H}'}{a^2} + \frac{\mathcal{H}^2}{a^2} \right) &= \frac{\delta_j^i}{a^2} \left[ 2\Phi'' + 4\mathcal{H}\Phi' + 2\mathcal{H}\Psi' + 2\Psi(2\mathcal{H}' + \mathcal{H}^2) - (1 + 4\Phi)\Delta\Phi - 2\delta^{mn}\Phi_{,m}\Phi_{,n} \right. \\ &\quad \left. + (1 + 2\Phi - 2\Psi)\Delta\Psi - \delta^{mn}\Psi_{,m}\Psi_{,n} \right] + \frac{\delta^{ik}}{a^2} \left[ (1 + 4\Phi)\Phi_{,jk} - (1 + 2\Phi - 2\Psi)\Psi_{,jk} \right. \\ &\quad \left. + B'_{(j,k)} + 2\mathcal{H}B_{(j,k)} + h''_{jk} + 2\mathcal{H}h'_{jk} - \Delta h_{jk} + \Psi_{,j}\Psi_{,k} - 2\Psi_{(j}\Phi_{,k)} + 3\Phi_{,j}\Phi_{,k} \right], \quad (4c) \end{aligned}$$

up to terms which are higher order corrections to our approximation scheme (cf. Appendix A of [26]). Here  $\mathcal{H}(\tau) = H(\tau)a(\tau) = a'/a$  is the comoving Hubble rate. For the time-time component (4a) and the spatial

trace of (4c), the FLRW background terms were moved to the left-hand side. Indices in parentheses are to be symmetrized.

The metric perturbations are sourced by the perturbations of the total stress-energy tensor  $T_{\mu}^{\nu}$ . It contains contributions from all types of matter, possibly a cosmological constant, and any other additional components one wants to include in a model. We will explicitly consider the contributions from nonrelativistic matter (baryons and cold dark matter) and a cosmological constant  $\Lambda$ , and

<sup>1</sup>We present the scheme from a slightly different point of view than [26], whose approach may be conceptually more elaborate but also more difficult to grasp. In particular, the weight of each term in the perturbative expansion is considered separately at small and large scales. The reader who is interested in a more detailed derivation of the equations is invited to study their accounts.

keep an unspecified remainder to collectively account for other sources of stress energy:

$$T_{\mu}^{\nu} = T_{m\mu}{}^{\nu} - \frac{\Lambda}{8\pi G} \delta_{\mu}^{\nu} + T_{X\mu}{}^{\nu}. \quad (5)$$

We do not distinguish between baryons and cold dark matter. In a perturbed universe, physical quantities like e.g. the energy density of matter are affected by the metric perturbations. Our aim is to take these corrections consistently into account when running a numerical simulation of structure formation. For convenience, we will therefore write the components of the matter stress-energy tensor in terms of “bare” quantities which can easily be computed in any standard  $N$ -body framework. In these frameworks, the phase space distribution of dark matter particles is usually sampled by a collection of test particles whose positions and peculiar velocities are followed through a simulation. By making a particle-to-mesh projection, it is possible to obtain average quantities like the (bare) bulk velocity  $u^i \doteq \langle v^i \rangle = \langle dx^i/d\tau \rangle$ , where  $\langle \cdot \rangle$  denotes the averaging procedure associated with the projection method. The method consists of a prescription of how to assign  $N$ -body particle properties, like mass or velocity, to nearby grid points, thus constructing a matter density and velocity field on the grid by means of a weighted average, see Appendix A 4 for more details. This can be considered as “the poor man’s equivalent” of a phase space integral.

We assume here that this procedure is carried out in the standard way without any knowledge about the perturbed metric, which is why we refer to bare quantities. Therefore, the projection gives rise to the bare rest mass density defined as

$$\rho \doteq \frac{\text{rest mass}}{\text{coordinate volume}} \times a^{-3}. \quad (6)$$

In terms of the bare quantities, the physical (dressed) energy density of matter reads

$$\rho_{\text{phys}} \doteq -T_{m0}{}^0 = \left[ 1 + 3\Phi + \frac{1}{2} \langle v^2 \rangle \right] \rho, \quad (7)$$

up to higher order corrections which we neglect. As one can see, our approximation scheme takes into account the leading corrections coming from the perturbation of the volume and the kinetic energy of the particles.

It should also be noted that even the homogeneous modes of  $\rho$  and  $\rho_{\text{phys}}$  do not agree in general, because the kinetic energy is strictly positive and hence has a positive average over the hypersurface of constant time. It is therefore necessary to specify more precisely how one wants to perform the split between background and perturbations. We decide to evolve the scale factor according to Friedmann’s equation using an exactly pressureless equation of state for cold dark matter (CDM), in the spirit of Newtonian  $N$ -body simulations. This means that we treat all finite velocity effects entirely on the level of the

perturbations. As we shall see later, this leads to a non-vanishing homogeneous mode in  $\Phi$ , which accounts for the correction to the scale factor<sup>2</sup> due to an effective pressure and other quadratic contributions. In fact, this correction can be interpreted as a backreaction term. However, as long as the homogeneous mode remains small, the scale factor  $a$  still gives a meaningful description of the background cosmology.

In short, for conceptual simplicity, we will use the bare  $\rho$  and  $\delta$  which one would infer from a given particle configuration assuming an unperturbed Friedmann model with scale factor  $a$ , but we have to keep in mind that these quantities have to be interpreted differently in the perturbed universe and have to be dressed with appropriate corrections when they enter the perturbed Einstein equations.

From  $G_0^0 = 8\pi G T_0^0$ , and using Friedmann’s equation, we obtain a first evolution equation for the metric:

$$\begin{aligned} (1 + 4\Phi)\Delta\Phi - 3\mathcal{H}\Phi' - 3\mathcal{H}^2\Psi + \frac{3}{2}\delta^{ij}\Phi_{,i}\Phi_{,j} \\ = 4\pi G a^2 \bar{\rho} \left[ \delta + 3\Phi(1 + \delta) + \frac{1}{2}(1 + \delta)\langle v^2 \rangle \right] \\ - 4\pi G a^2 \delta T_{X0}{}^0. \end{aligned} \quad (8)$$

Here,  $\delta T_{X0}{}^0 \doteq T_{X0}{}^0 - \bar{T}_{X0}{}^0$ , where  $-\bar{T}_{X0}{}^0$  and  $\bar{\rho}$  are the homogeneous modes of the energy densities as they occur in Friedmann’s equation. In particular,

$$4\pi G \bar{\rho} = \frac{3}{2} H_0^2 \Omega_m (1 + z)^3, \quad (9)$$

with  $H_0$ ,  $\Omega_m$ , and  $z$  being bare parameters of the FLRW background. The Poisson equation (2) is obtained from Eq. (8) by dropping all terms except the first one on each side.

One can view Eq. (8) as a parabolic (diffusion-type) equation for  $\Phi$  to which Eq. (2) is a first approximation if the diffusion time scale  $t_{\text{diff}}$  is much shorter than the dynamical time scale  $t_{\text{dyn}}$  of the source term. To illustrate this statement, let us consider a structure of size  $r$  consisting of nonrelativistic matter. A quick estimate gives<sup>3</sup>

$$\frac{t_{\text{diff}}}{t_{\text{dyn}}} \simeq \frac{r^2}{r_H^2} \sqrt{1 + \delta}, \quad (10)$$

where  $r_H = a\mathcal{H}^{-1}$  is the Hubble radius, and we use the free-fall time  $\simeq r_H/\sqrt{1 + \delta}$  as an indicator for  $t_{\text{dyn}}$ .

<sup>2</sup>A homogeneous mode in  $\Psi$  on the other hand can be gauged away by a global reparametrization of time. We will take the conventional definition of cosmic time by imposing that  $\Psi$  has a vanishing homogeneous mode.

<sup>3</sup>As diffusion is a random process, the diffusion length is proportional to  $\sqrt{\kappa t}$  where  $\kappa = a/(3\mathcal{H})$  is the diffusion coefficient that can be read off from the prefactors of  $\Delta\Phi$  and  $\dot{\Phi} = a\Phi'$  in Eq. (8). The diffusion time scale for a structure of size  $r$  is then  $t_{\text{diff}} = r^2/\kappa$ .

This ratio is tiny for any realistic structure with  $r \ll r_H$ . For instance, plugging in typical numbers for a stellar object yields  $t_{\text{diff}}/t_{\text{dyn}} \sim 10^{-20}$ , while for a structure comparable to the local supercluster one obtains  $t_{\text{diff}}/t_{\text{dyn}} \sim 10^{-5}$ . This means that  $\Phi$  will simply adjust adiabatically to its ‘‘instantaneous’’ equilibrium solution on these scales, which is why Eq. (2) is a reasonable approximation in this case. On cosmological scales  $r \simeq r_H$ , however, one may expect that retardation effects may become relevant. Furthermore, gauge dependence typically becomes an issue as well on these scales, even in the linear regime. In our case this leads, for instance, to the  $\mathcal{H}^2\Psi$  term present in Eq. (8) which does not appear in Poisson’s equation.

In order to obtain a second scalar equation, it is useful to combine the time-time components and spatial trace in the following way:

$$\frac{a^2}{2} \left( G_i^i - 3G_0^0 - \frac{1}{\mathcal{H}} G_0^{0'} \right) = 4\pi G a^2 \left( T_i^i - 3T_0^0 - \frac{1}{\mathcal{H}} T_0^{0'} \right). \quad (11)$$

Since  $T_\mu^\nu$  is covariantly conserved, one can replace  $T_0^{0'}$  essentially by spatial derivatives of the stress-energy tensor, which are more easily computed at every time step of a simulation. After some algebra and using again Friedmann’s equations, one arrives at

$$\begin{aligned} & (1 + 2\Phi - 2\Psi)\Delta\Psi - \delta^{ij}\Psi_{,i}(\Phi_{,j} + \Psi_{,j}) \\ & + \frac{1}{\mathcal{H}}(\Delta\Phi' + 4\Phi\Delta\Phi' + 4\Phi'\Delta\Phi) + \frac{3}{\mathcal{H}}\delta^{ij}\Phi'_{,i}\Phi_{,j} \\ & = 4\pi G \frac{a^2}{\mathcal{H}} \left[ -\bar{\rho}(1 + 3\Phi)((1 + \delta)\langle\gamma v^i\rangle)_{,i} \right. \\ & - \bar{\rho}(1 + \delta)u^i\Psi_{,i} + 3\bar{\rho}\Phi'\delta + \delta T_{X0,i}^i \\ & - \delta T_{X0}^i(3\Phi_{,i} - \Psi_{,i} + B'_i) - \Phi'(3\delta T_{X0}^0 - \delta T_{Xi}^i) \\ & \left. - \frac{1}{2}\delta^{ik}h'_{jk}\delta T_{Xi}^j \right], \quad (12) \end{aligned}$$

up to terms which we neglect in our approximation scheme. Here, because a spatial derivative acts on it, we have to use the relativistic momentum up to cubic order in velocity, i.e. we take into account the Lorentz factor which we approximate to quadratic order,  $\gamma \simeq 1 + v^2/2$ . Dropping again all terms except the first one on either side gives a Poisson equation for  $\Psi$  which, however, is sourced by the divergence of the momentum density instead of the density perturbation which we had in Eq. (2). Of course these two are related by the continuity equation, and hence the two expressions are the same to a first approximation, e.g. for linear perturbations of CDM.

In Eqs. (8) and (12) we make no assumptions about the size of the perturbations  $\delta T_{X\mu}^\nu$ , so they can be used to obtain the scalar metric perturbations  $\Phi$ ,  $\Psi$  in any setting where these stress-energy terms can be reliably computed, whatever their origin may be.

Note also that Eq. (8) is a purely scalar equation. Moreover, whenever the two terms  $\delta T_{X0}^i B'_i$  and  $\delta^{ik}h'_{jk}\delta T_{Xi}^j$  can be neglected, also Eq. (12) decouples from vector and tensor perturbations. In a numerical simulation, one can then solve these equations first and use the solutions in order to solve for the vector and tensor quantities separately. This is the approach we will follow in Sec. III, where we discuss the implementation of this scheme for a pure ( $\Lambda$ )CDM universe (where  $\delta T_{X\mu}^\nu = 0$ ). The equations are, of course, still coupled indirectly by the evolution of  $T_\mu^\nu$ .

The equation for vector perturbations is

$$\begin{aligned} & -\frac{1}{4}\Delta B_i - \Phi'_{,i} - \mathcal{H}\Psi_{,i} \\ & = 4\pi G a^2 [\bar{\rho}(1 + \delta)(\delta_{ij}u^j - B_i) + \delta T_{Xi}^0]. \quad (13) \end{aligned}$$

Note that the left-hand side is already written in Helmholtz decomposition and that the longitudinal component of the equation is completely determined by  $\Phi$  and  $\Psi$ . On the other hand, by taking the curl of it, we could get rid of the scalar potentials. However, the nonlinear term  $\delta \cdot u^j$  remains and the term  $\delta \cdot B_i$  prevents us from writing an equation for the curl of  $B_i$  only. Therefore, we prefer to solve Eq. (13) directly after subtracting its longitudinal component through the use of  $\Phi$  and  $\Psi$  (see also Sec. III B for more details on how we do this in practice).

Finally, in order to obtain an equation for the tensor perturbations, it is useful to consider the traceless combination

$$G_j^i - \frac{1}{3}\delta_j^i G_k^k = 8\pi G \left( T_j^i - \frac{1}{3}\delta_j^i T_k^k \right), \quad (14)$$

which yields<sup>4</sup>

$$\begin{aligned} & h''_{ij} + 2\mathcal{H}h'_{ij} - \Delta h_{ij} + B'_{(i,j)} + 2\mathcal{H}B_{(i,j)} + (1 + 4\Phi)\Phi_{,ij} \\ & - (1 + 2\Phi - 2\Psi)\Psi_{,ij} + \Psi_{,i}\Psi_{,j} - 2\Phi_{,i}\Psi_{,j} \\ & + 3\Phi_{,i}\Phi_{,j} - \frac{1}{3}\delta_{ij}[(1 + 4\Phi)\Delta\Phi \\ & - (1 + 2\Phi - 2\Psi)\Delta\Psi + \delta^{mn}\Psi_{,m}\Psi_{,n} \\ & - 2\delta^{mn}\Psi_{,m}\Phi_{,n} + 3\delta^{mn}\Phi_{,m}\Phi_{,n}] \\ & = 8\pi G a^2 \left[ \bar{\rho}(1 + \delta)\pi_{ij} + \delta_{ik}\delta T_{Xj}^k - \frac{1}{3}\delta_{ij}\delta T_{Xk}^k \right]. \quad (15) \end{aligned}$$

Here,  $\pi_{ij}$  is the bare anisotropic stress of matter, defined as  $\pi_{ij} \doteq \delta_{im}\delta_{jn}\langle v^n v^m \rangle - \delta_{ij}\langle v^2 \rangle/3$ . Again, taking a double curl would remove the vector and the linear scalar contributions. But since there are many nonlinear scalar terms which survive, this does not seem promising.

<sup>4</sup>In Eqs. (A2) and (A4) of [26] they include a contribution from  $B_i$  on the right-hand side, which to our understanding should be dropped because it is multiplied by a velocity and hence is of higher order in the approximation scheme.

The system of equations is closed once the equations of motion for all sources of stress-energy are specified. For CDM particles the evolution of their phase space distribution follows from the geodesic equation of massive (nonrelativistic) particles, given by

$$\frac{d^2 x^i}{d\tau^2} + \mathcal{H} \frac{dx^i}{d\tau} + \delta^{ij} \left[ \Psi_{,j} - B'_j - \mathcal{H} B_j + 2B_{[j,k]} \frac{dx^k}{d\tau} \right] = 0, \quad (16)$$

up to corrections beyond our approximation. Indices in square brackets are to be antisymmetrized. In a pure ( $\Lambda$ )CDM simulation,  $T_{X\mu}{}^\nu = 0$ , the tensor perturbations  $h_{ij}$  do not feed back into the evolution of  $T_{\nu}{}^\mu$  within our approximation. Therefore, as long as one does not want to extract the tensor signal, the system of equations can be closed without considering Eq. (15). Of course, not all observables can then be reconstructed consistently, as  $h_{ij}$  occurs for instance in the null geodesic equation for light rays.

Interacting massive particles, like baryons, do not follow exact geodesics due to additional forces acting on them. These forces have to be modeled according to the relevant microphysics. In this paper we do not concern ourselves with this problem which is mainly relevant on small scales.

### III. NUMERICAL IMPLEMENTATION

In this section we discuss in some more detail what it takes to convert a state-of-the-art Newtonian  $N$ -body code into a general relativistic one in the sense of our approximation scheme, which is particularly tuned for cosmological applications.  $N$ -body simulations have a long history alongside advancements in super computing technology, and it is beyond the scope of this paper to give a comprehensive review of the subject. Some useful references are [33–36]. Further references can be found therein.

The  $N$ -body problem refers to the dynamics of  $N$  particles which interact through long range forces. There are essentially two ways to address the problem. One possibility is to consider the force acting on each particle as a sum of two-body forces, which leads to the so-called “particle-to-particle” class of  $N$ -body algorithms. The alternative, referred to as the “particle-to-mesh” approach, is to construct a force field which permeates the entire volume of the simulation. To this end, one projects the particle configuration onto a 3D grid (representing position space) and thus generates a discretized density field. This grid information is used to compute the gravitational potential according to a discretized version of Eq. (2). The particles are then accelerated by the gradient of the potential, again suitably discretized and interpolated to the particle positions. Based on these two approaches, many highly sophisticated algorithms have been developed. There also exist algorithms,  $P^3M$  for example, which use a combination of both approaches.

In GR, gravitational interaction is mediated by the space-time metric. Therefore, it fits naturally into the framework of the particle-to-mesh approach. Instead of constructing the Newtonian gravitational potential, however, we have to deal with a multicomponent field, the metric, which determines the gravitational acceleration according to Eq. (16). In this paper, we discuss numerical solvers which allow one to obtain the metric components on a structured mesh. These can then be implemented in any suitable existing  $N$ -body code, which takes care of all remaining tasks, like parallelization and mesh management.

From now on, we assume  $\delta T_{X\mu}{}^\nu = 0$ . That is, we develop a relativistic  $N$ -body algorithm for a standard  $\Lambda$ CDM model. In this context, it is expected that Newtonian codes already give accurate results. On small scales, there is a broad consensus on this. But on large scales, in particular scales which are outside the horizon when the initial conditions are laid down, this is still under debate. Already within linear perturbation theory there are relativistic corrections and the gauge dependence of the variables is important on super horizon scales [7,8,37,38].

Large-volume simulations will be important for the future large cosmological surveys, and so, not surprisingly, the horizon scale has already been crossed in recent Newtonian simulations. Examples are the Millennium simulation [35], the Hubble Volume Project [39,40], the Marenstrum Numerical Cosmology Project [41], and others [42]. It will be interesting to compare them with our semirelativistic approach and we think that this will provide a useful test of the validity of the Newtonian treatment on cosmological scales. Furthermore, we hope to be able to give robust statements about the actual size of relativistic corrections. In order to study extensions or alternatives to the standard model, the numerical scheme will have to be amended for an appropriate treatment of  $\delta T_{X\mu}{}^\nu \neq 0$ .

Let us now briefly sketch the main components of our algorithm. At all times, the state of the system, representing Cauchy data on a hypersurface of constant time which we may call a “snapshot of the Universe,” is stored in two sets of data: a particle list containing positions  $x^i$  and peculiar velocities  $v^i = dx^i/d\tau$  of  $N$  test particles which are used to sample the phase space distribution function<sup>5</sup> of CDM, and a 3D grid (representing position space) holding values of all relevant fields at each grid point. A standard particle-to-mesh projection allows one to construct, from the particle list, the relevant moments of the CDM distribution function on the grid, which we have defined as the bare quantities  $\rho$ ,  $u^i$ , and  $\pi_{ij}$ . Some details on how this construction works can be found in Appendix A.

<sup>5</sup>Unfortunately, representing the full distribution function of CDM in six-dimensional (discretized) phase space is prohibitive, which is why the concept of test particles has to be introduced in the first place.

Instead of merely solving for the Newtonian potential as in a Newtonian particle-to-mesh code, we solve discretized (grid-based) versions of Eqs. (8), (12), and (13), and possibly (15). The grid-based representation of the metric, suitably interpolated to the particle positions (see Appendix A), is then used to evolve the particle list by an infinitesimal time increment according to the geodesic equation (16), after which a next particle-to-mesh projection is performed in order to update the metric, and so on.

In principle, our  $N$ -body scheme does not look very different from the Newtonian one. The equation for the particle acceleration is slightly modified, and instead of an algorithm which solves the elliptic Poisson equation (2), we need to implement algorithms which solve Eqs. (8), (12), and (13), and possibly (15). With  $\delta T_{X\mu}{}^\nu = 0$ , Eqs. (8) and (12) do not depend on  $B_i$  or  $h_{ij}$  directly, so a natural ordering is to use them to obtain solutions for the scalar perturbations  $\Phi$  and  $\Psi$ , which can later be plugged into the vector equation (13). Similarly, the vector perturbation  $B_i$  can then be determined without any knowledge of  $h_{ij}$ , and all the solutions can finally be used in Eq. (15) to solve for the tensor perturbations. Let us now discuss possible algorithmic solutions of these equations, one at a time.

### A. The scalar equations

The two scalar equations (8) and (12) form a coupled system which is first order in time for  $\Phi$ , but contains no time derivatives of  $\Psi$ . It is important to note that these equations are in fact a set of constraints, since  $\Phi$  and  $\Psi$  themselves are not independent dynamical degrees of freedom. From their constrained dynamics we expect that they evolve only very slowly, much slower even than the motion of individual  $N$ -body particles, for instance. It is therefore sufficient, as a first approach, to construct a numerical update scheme which is only first order accurate in time. This approach has the advantage that one can very easily decouple the update of  $\Phi$  and  $\Psi$ : we will use Eq. (8) to update  $\Phi$ , using the known  $\Psi$  of the previous time step. The new  $\Phi$  and  $\Phi'$  obtained from this update step can then be used in Eq. (12) to find a new solution for  $\Psi$ .

Under these premises, Eq. (8) is a nonlinear parabolic equation for  $\Phi$  with a given source. If we forget about the nonlinearity for a moment (which is anyway expected to remain very weak), it resembles a diffusion equation. This type of mathematical problem is very well studied and can be solved with various standard methods found in the literature, see e.g. [43–45].

The methods basically differ in the way the differential operators are discretized, and the choice can have a tremendous impact on the performance of the algorithm. For instance, a fully explicit scheme is unstable unless the time step  $d\tau$  satisfies a so-called Courant-Friedrichs-Lewy condition, which essentially states that information may not travel by more than one lattice unit within one time step. For our equation,  $\Phi$  information will basically propagate at

the speed of light, while on the other hand, particle velocities are roughly 3 orders of magnitude smaller. Therefore, it would take some thousand iterations before a particle would have traveled only across a single cell of the lattice. This drawback can be overcome by using implicit schemes, which can be shown to be unconditionally stable, hence allowing for much larger time steps. Since we violate the Courant-Friedrichs-Lewy condition of the explicit scheme, time resolution now becomes too coarse to follow the time evolution of the small scales correctly, and different schemes show different behavior on these scales. We will choose a scheme for which the small scales are driven towards their equilibrium solution ( $\Phi' \rightarrow 0$ ), because this corresponds to the behavior one expects from our discussion following Eq. (10).

Our choice is to use a slightly modified version of the alternating direction implicit (ADI) method described in [44]. There, an operator splitting method is used to construct an update rule which consists of three steps, i.e. one for each space dimension. In each step, an implicit set of equations has to be solved along a different spatial direction. For a linear parabolic operator, it can be shown that this algorithm is stable. We modify this method slightly by adding the nonlinear terms, similar to how it is done in [45]. Since the nonlinear terms are expected to remain subdominant, this will not affect the stability of the algorithm. More details, including the discretized version of Eq. (8), can be found in Appendix A.

In order to perform a single update step from  $\tau$  to  $\tau + d\tau$  within the ADI framework, one has to invert a tridiagonal matrix for each “line” of grid points along the implicit direction. This can be done efficiently using the Thomas algorithm, which is easily parallelized for supercomputing applications [46]. In fact, the numerical solution of Eq. (8) with this method is computationally not more expensive than solving the Poisson equation (2) with the Fourier method. Since the ADI method operates in position space (rather than Fourier space), it is also compatible with adaptive mesh refinement, which is a widely used approach to effectively increase the resolution of a simulation. We are therefore confident to obtain a high performance of the algorithm within any state-of-the-art particle-to-mesh framework, competitive with the standard Poisson solvers which are used in Newtonian codes.

Next we construct a new solution for  $\Psi$  with the help of Eq. (12). Having already computed  $\Phi$  and  $\Phi'$ , this is a nonlinear elliptic equation for  $\Psi$  with known coefficients and source. It can be solved again by standard methods, for instance using a multigrid algorithm coupled to a nonlinear Gauß-Seidel relaxation scheme [43]. Again, particular details can be found in Appendix A. This approach should also compare well to the performance of a Newtonian code.

Having to solve two equations, (8) and (12), both requiring a numerical effort comparable to the simple Poisson equation (2), the relativistic simulation will accordingly be

somewhat more expensive, but this is of course to be expected when we solve for two fields instead of one.

### B. The vector equation

Let us now discuss how to obtain a solution for the vector perturbation  $B_i$ , for given solutions  $\Phi$  and  $\Psi$ . We use Eq. (13), which is a linear elliptic equation for  $B_i$ . Because of the product with the density perturbation on the right-hand side, we use a method which operates in position space, multigrid relaxation being an obvious possibility. We also have to avoid that numerical errors drive the solution away from the transverse gauge. This can be done by subtracting the spurious longitudinal component from the solution. It is given by the gradient of a scalar function  $\chi$  which solves  $\Delta\chi = \delta^{ij}\tilde{B}_{i,j}$ , where  $\tilde{B}_i$  is a numerical solution with spurious longitudinal component. One then has  $B_i = \tilde{B}_i - \chi_{,i}$ . All together, finding the solution  $B_i$  amounts to solving four linear elliptic equations (one for each component of  $\tilde{B}_i$  and one for  $\chi$ ) which are of the same numerical difficulty as Poisson's equation.

If one is not interested in the signal from tensor perturbations (gravitational waves), one can now close the loop by implementing a particle update according to a suitable discretization of the geodesic equation (16). This is possible because  $h_{ij}$  does not occur in the geodesic equation of massive particles at the level of our approximation. Otherwise, one has to finally proceed with Eq. (15).

### C. The tensor equation

Having solutions for  $\Phi$ ,  $\Psi$ , and  $B_i$  in hand, Eq. (15) is a linear wave equation for the tensor modes  $h_{ij}$  with a given source. Since it is linear, the different modes decouple in Fourier space where we are effectively dealing with an ordinary differential equation (ODE) per Fourier-grid point. In addition, the gauge condition can be easily implemented in Fourier space. However, the hyperbolic nature of the equation means that in principle we would need a very high resolution in time in order to resolve the rapid oscillations of the high-momentum waves that travel at the speed of light.

This problem could be approached with the help of a standard stiff ODE solver, but we can gain more insight into the behavior of the tensor modes by using a Green's function method: In a  $\Lambda$ CDM setup the source is given only by nonrelativistic matter. Therefore, the rapid oscillations come entirely from the homogeneous part of the equation while the source term varies only slowly. Given the homogeneous solutions in Fourier space,  $h_{(1)}(\tau)$  and  $h_{(2)}(\tau)$ , one easily obtains the solution with source term by performing the integral,

$$h(\tau) = \int_{\tau_{\text{in}}}^{\tau} \frac{h_{(1)}(\tau)h_{(2)}(\tau') - h_{(1)}(\tau')h_{(2)}(\tau)}{W(\tau')} S(\tau') d\tau', \quad (17)$$

where  $W \doteq h_{(1)}h'_{(2)} - h'_{(1)}h_{(2)}$  is the Wronskian of the free solutions  $h_{(1)}$  and  $h_{(2)}$ , and  $h(\tau)$  is the driven solution with

vanishing initial values at  $\tau_{\text{in}}$ , which is what we need. Here we have suppressed the tensor indices in  $h$  and in the source but these are trivial in Fourier space.

In the matter dominated era, at redshift  $z \gtrsim 2$ , we can directly write down the homogeneous solutions. They are simply given by spherical Bessel functions,  $h_{(1)} = (k\tau)^{-1}j_1(k\tau)$  and  $h_{(2)} = (k\tau)^{-1}y_1(k\tau)$ , with Wronskian  $W = k/(k\tau)^4$ .

As is evident from the above expression, the oscillations are only driven when the frequency of the source term approximately matches the one of the Green's function, which (for a nonrelativistic matter source) happens only close to horizon crossing. At very much slower variation of the source, the behavior of the system becomes that of a damped oscillator whose rest position adiabatically follows a slowly varying external force. This means, as soon as the oscillations have died away, the displacement of the oscillator is simply proportional to the instantaneous force. In addition to this contribution which is sourced inside the horizon, we have free gravitational waves which have been produced at horizon crossing, with energy density scaling as  $\rho_h(k, \tau) \propto a^{-4}$ .

## IV. PLANE-SYMMETRIC CLUSTERING

In order to test essential parts of our algorithm without needing to run many simulations on a supercomputer, we restrict ourselves in this paper to the numerical simulation of plane-symmetric configurations. The planar symmetry trivializes two of the three spatial dimensions, which reduces the computational requirements dramatically. However, it should be stressed that imposing this symmetry is quite a strong restriction which precludes us from studying realistic models of cosmology. Furthermore, the allowed configurations do not contain vector or tensor modes by construction. The results presented here should therefore be understood as numerical tests of the algorithms, and can only be indicative of what will happen in more realistic situations. We shall extend our investigation to the full three-dimensional case in forthcoming work.

As a first case, we consider an Einstein–de Sitter background with an initial perturbation which is given by a single plane wave with a comoving wavelength of  $100 \text{ Mpc}/h$ .

We initialize the simulation at  $z \simeq 5000$  using the linear solution with an amplitude of  $\Phi = \Psi = 1.5 \times 10^{-4}$ , which is quite large in the sense that it will finally result in particle velocities which reach  $\sim 1\%$  of the speed of light. The generation of initial conditions in our general relativistic approach has to be done in a slightly different way than for Newtonian simulations, in order to correctly account for gauge dependencies. Details are given in Appendix B.

Results are shown in Fig. 1. The fluctuation first grows linearly, but at  $z = 3$  has reached a nonlinear density contrast of  $\delta \sim 10$ . Eventually, at  $z = 0$ , two shell

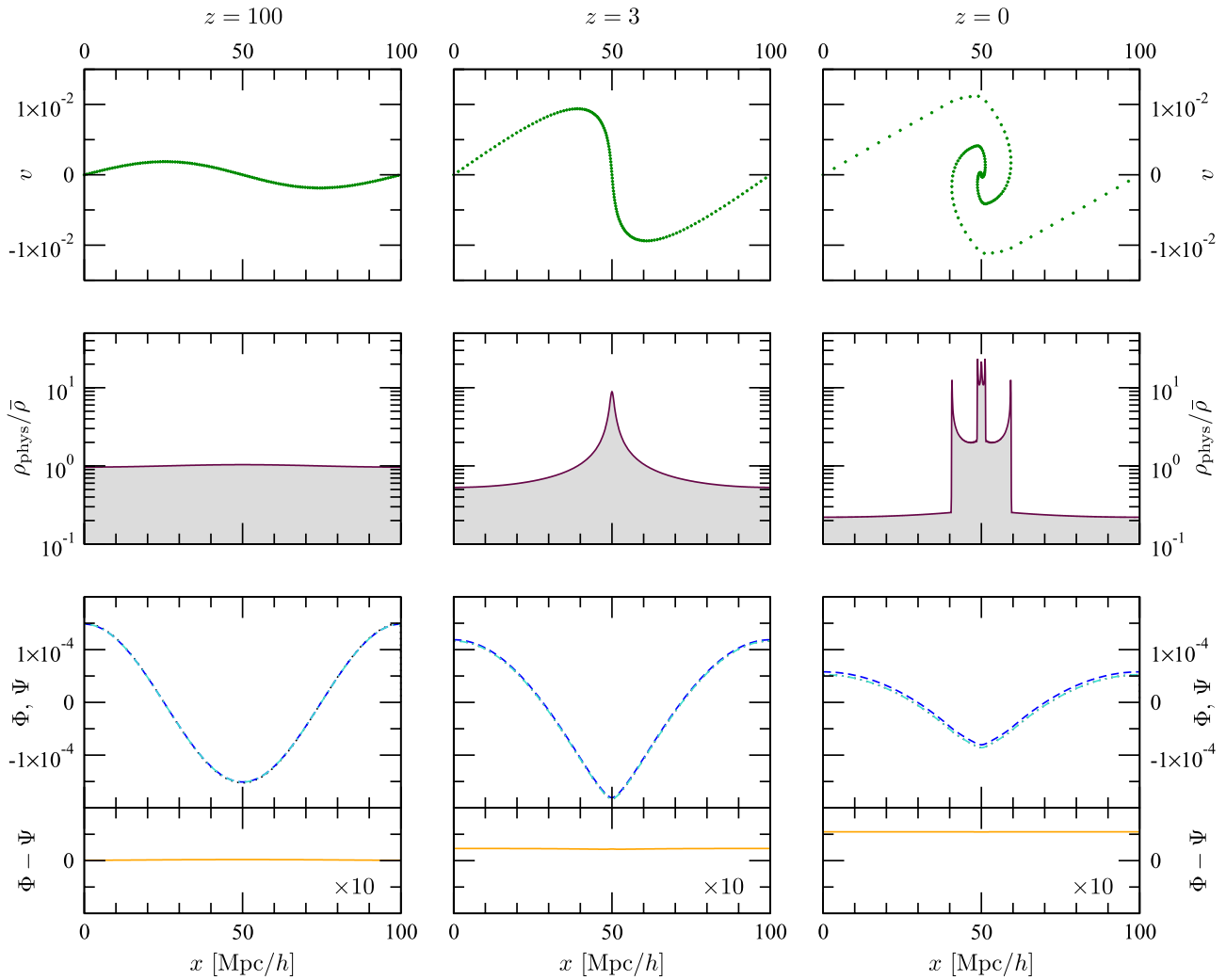


FIG. 1 (color online). The plane wave example: the  $x$  axis always refers to the nontrivial spatial direction and is given in comoving units. The three columns show snapshots at three different redshifts,  $z = 100$  (perturbations are still linear),  $z = 3$  (the density perturbation is becoming nonlinear), and  $z = 0$  (today). The first row depicts the particle phase space of the simulation, it is easy to see how shell crossing leads to a spiral-like structure in  $(x, v)$ . In the second row we plot the density. As the central region around  $x = 50$  Mpc/h is overdense, this region undergoes gravitational collapse, resulting eventually in shell crossing and the associated formation of caustics visible as sharp spikes at  $z = 0$ . The bottom row shows the behavior of the gravitational potentials  $\Phi$  (dark blue dashed line) and  $\Psi$  (light blue dot-dashed line). We see that in this example the potentials always remain small, of the order of the initial value of  $10^{-4}$ . To display the difference between the potentials more clearly, we plot it multiplied by a factor of 10 in the bottom-most panel (using otherwise the same scale as for the potentials). This difference mainly consists of a homogeneous mode that can be interpreted as a correction to the background scale factor due to nonlinear effects. The simulation was carried out with a resolution of 1024 grid points and 16384 particles (a representative subset is shown in the phase space diagram).

crossings have occurred, which are highly nonlinear effects. As one can see on the bottom panel, the two relativistic potentials  $\Phi$  and  $\Psi$  agree extremely well, up to the homogeneous mode in  $\Phi$  which reaches an amplitude of  $\sim 5 \times 10^{-6}$  at  $z = 0$ .

The amplitude of the homogeneous mode of  $\Phi$  agrees well with our naive expectation that it should be governed by  $v^2$ . However, its precise value could not have been computed simply by averaging  $v^2$  from a Newtonian simulation and dressing Friedmann's equations with a corresponding effective pressure and energy density. This is

because other quadratic terms occur in the equations, like  $\delta^{ij}\Phi_{,i}\Phi_{,j}$ , which are of the same order as  $v^2$  and also contribute to the generation of the homogeneous mode.

As a second case, we study a plane-symmetric setup inspired by the  $\Lambda$ CDM cosmology. Since a cosmological constant is a homogeneous source of stress energy, its effect enters the dynamics of cosmological perturbations only through a modification of the background. We choose a  $\Lambda$ CDM background with  $\Omega_\Lambda = 1 - \Omega_m \simeq 2/3$  and draw a Gaussian random sample of initial plane wave perturbations which are supposed to mimic a typical linear power

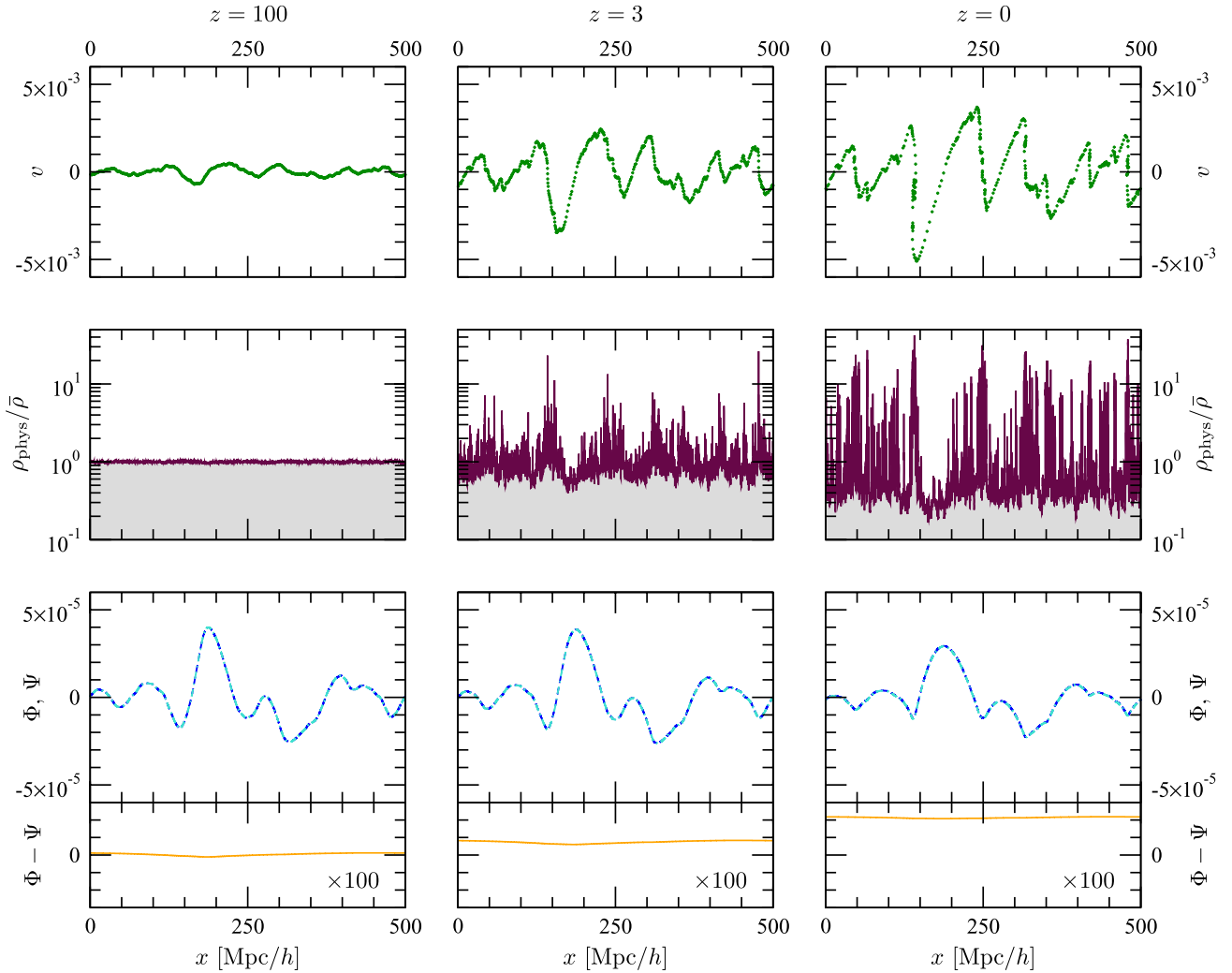


FIG. 2 (color online). A  $\Lambda$ CDM toy setup with planar symmetry:  $\Omega_\Lambda \approx 2/3$ , and the initial power spectrum for  $\Phi$  is flat for  $k < 0.075 h/\text{Mpc}$  and scales like  $k^{-4}$  for higher wave numbers. As in Fig. 1 we show the phase space (top row), the density (middle row), and the gravitational potentials (bottom row), for three different redshifts. The last panel shows  $\Phi - \Psi$  on the same scale as the potentials, but multiplied by a factor of 100 (as indicated in the panel). The difference consists again mostly of a homogeneous mode as in the plane wave example. The simulation was carried out with a resolution of 16384 grid points and contained 131072 particles.

spectrum of standard cosmology. However, as opposed to the standard case of an isotropic power spectrum, our plane symmetry forces us to only include perturbations whose wave vector is perpendicular to the plane of symmetry. Therefore, in order to obtain the right amplitude of perturbations at each scale, we choose  $k\langle|\Psi_k|^2\rangle \propto k^3 P(k)$ , where  $P(k)$  denotes the usual isotropic linear power spectrum. Conversely, when quoting results for the power spectra, we perform the angular integration over all wave vectors as if the perturbations were statistically isotropic.

We choose an initial power spectrum where  $k^3 P(k)$  is constant (scale invariant) at scales  $k < 0.075 h/\text{Mpc}$  and decays as  $k^{-4}$  on smaller scales. The simulation is initialized at  $z = 3900$  using linear theory, which in the real Universe would be at the transition between radiation and matter domination. However, in our toy setup we do not

include any radiation. Linear theory guarantees that the linear solution will be in the growing mode (of the matter dominated solution) after a couple of Hubble times, which means that radiation effects, for the purpose of CDM simulations, can be taken into account simply by adjusting the amplitude of the growing mode. The physics of the radiation era and the transition to matter domination are contained in the shape of the linear power spectrum.

Results are plotted in Figs. 2 and 3. As in the previous example, we see that the difference  $\Phi - \Psi$  is dominated by the homogeneous mode of  $\Phi$ . The nonhomogeneous ( $k \neq 0$ ) component of  $\Phi - \Psi$  has a very red spectrum. Since we are in a setup where the “dictionary” of [26], given by their equations (2.40)–(2.42), should be valid, we can actually estimate this component by computing a correction  $\xi \doteq (\Psi - \Phi)_{k \neq 0}$  with the help of their

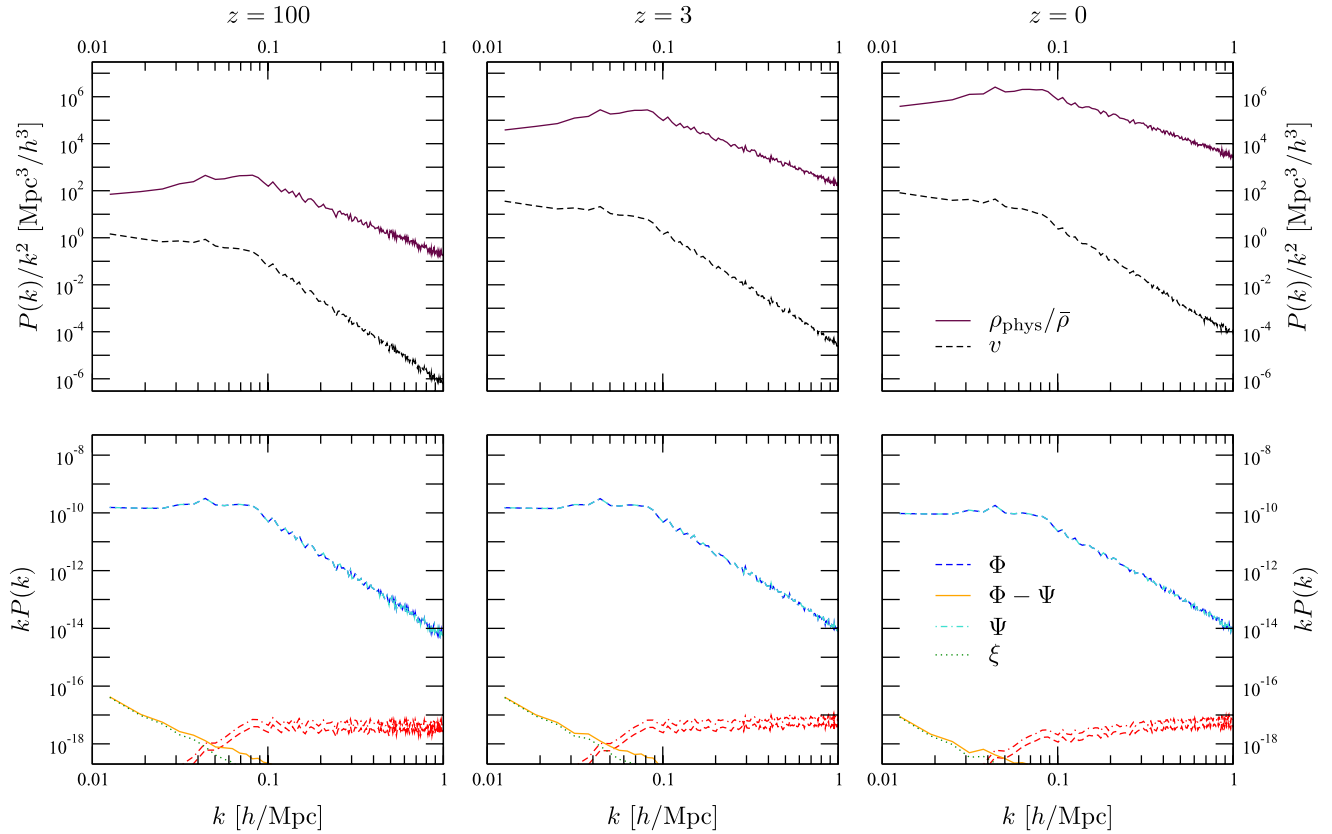


FIG. 3 (color online). Power spectra averaged over 50 realizations of the  $\Lambda$ CDM toy setup for three different redshifts. The upper panels show the power spectra of the density (solid line) and of the velocity perturbations (dashed line). In the lower panels we plot the power spectra of the gravitational potentials  $\Phi$  (dark blue dashed line) and  $\Psi$  (light blue dot-dashed line) as well as their difference (orange solid line) compared to the second-order estimate (green dotted line) based on  $\xi$  from [26]. The red curves on the bottom of the plot show the truncation error (see text for definition) of the gravitational potentials and indicate the expected numerical accuracy, and hence the level to which we can trust  $\Phi - \Psi$ . Each simulation of the ensemble was carried out with a resolution of 4096 grid points and contained 32768 particles.

equation (3.17), where  $\Delta^2 \xi$  is given by a combination of quadratic terms in the velocity and in gradients of the Newtonian potential. To this end, we first obtain the Newtonian quantities present in the latter equation by applying the dictionary in the reverse direction. As one can see, the result obtained by this prescription agrees extremely well with our numerical result on the scales where it can be trusted.

The limited resolution introduces an intrinsic uncertainty in the numerical solutions for  $\Phi$  and  $\Psi$  on small scales. A benefit of the multigrid scheme is that the size of this uncertainty can easily be estimated: we compare each solution at full resolution with the one at half the resolution, interpolated to full resolution. The spectrum of the difference, the so-called truncation error, is seen at the bottom of each plot in the lower panel of Fig. 3 (for both  $\Phi$  and  $\Psi$ ). Certainly, the value of the potentials should only be trusted up to the level indicated by this truncation error, and so should the value of  $\Phi - \Psi$ . Because the difference between the potentials is so small, and has a red spectrum, it drops below the numerical accuracy on small scales.

As explained in Sec. II, the homogeneous ( $k = 0$ ) mode of  $\Phi$  can be regarded as a correction to the scale factor due to nonlinearities, and as such is a genuine backreaction effect. Its amplitude is governed by  $v^2$  and hence grows during linear evolution roughly  $\propto a$ , as can be seen for our two numerical examples in Fig. 4. However, as mentioned earlier, its value can only be computed consistently by taking into account all contributions at a given order of approximation. At order  $v^2$  there are, for instance, also terms like  $\delta^{ij} \Phi_{,i} \Phi_{,j}$  which are relevant.

In order to assess further the difference between the traditional Newtonian approach and our general relativistic one, we also run a purely Newtonian simulation which is initialized on the identical linear solution as the example of Fig. 2. We then perform the following comparison between the two simulations: on the initial data, before applying the initial infinitesimal displacements, each  $N$ -body particle of the Newtonian simulation is paired with the corresponding  $N$ -body particle of the relativistic simulation. Since the scalar velocity perturbation is gauge invariant, their initial velocities match perfectly; on the other hand, as explained

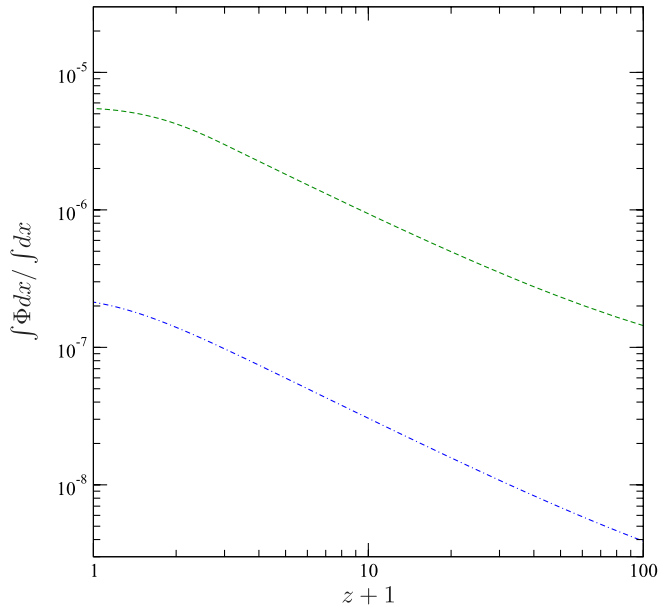


FIG. 4 (color online). The homogeneous mode of  $\Phi$  for the plane wave setup (green, dashed) and the  $\Lambda$ CDM setup (blue, dot-dashed). This homogeneous mode shows the size of the backreaction effect for the plane-symmetric case, i.e. the amount by which the average evolution of the perturbed universe differs from the exact FLRW solution. More precisely, it can be absorbed into the background by a redefinition  $a \rightarrow a(1 + \int \Phi dx / \int dx)$ .

in Appendix B, the initial particle displacement is gauge dependent and consequently does not show perfect agreement. At  $z = 0$ , however, the entire simulation box is well inside the particle horizon, and one therefore expects gauge dependence to be weak. Preserving the initial pairing of particles, they are followed through the two separate simulations. Figure 5 shows the separation of particle pairs in terms of phase space coordinates at  $z = 100$ ,  $z = 3$ , and  $z = 0$ . Evidently, the  $N$ -body particles remain highly correlated between the two simulations. The rms separation in position space rises from  $\sim 2.5$  kpc/ $h$  (comoving) in the initial data to  $\sim 3.2$  kpc/ $h$  at  $z = 0$ , where the rms velocity difference reaches  $\sim 10^{-6}$ .

This excellent agreement demonstrates that nonlinear effects of GR, at least when confined to the scalar sector, have an almost negligible effect on the evolution of the  $N$ -body particle ensemble. On large scales where particle displacements can be computed perturbatively, a similar level of agreement was found in [28]. Our results give a quantitative indication that it extends to all scales on which gravitational fields remain weak, even if the particle distribution becomes highly nonlinear. This underlines the sound performance of the Newtonian approximation. Note that the grid resolution of the two simulations was  $\sim 30$  kpc/ $h$ , which means that corresponding particles of the Newtonian and relativistic simulation are basically all found within the same grid cell.

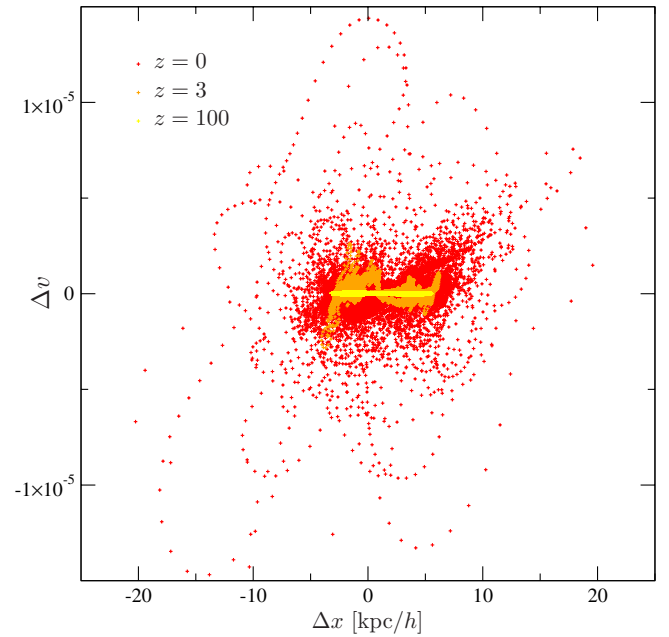


FIG. 5 (color online). Difference of the phase space coordinates for  $N$ -body particles in the relativistic simulation of Fig. 2 and a purely Newtonian one, initialized on the same linear solution. The three colors yellow, orange, and red correspond to redshifts  $z = 100$ ,  $z = 3$ , and  $z = 0$ , respectively. As long as the solution is in the linear regime (yellow,  $z = 100$ ), the difference in particle positions is essentially due to gauge dependence. At later times, however, particle positions and velocities become affected by relativistic corrections. Nevertheless, the phase space distribution of particles for the two different simulation techniques remains highly correlated, with velocities in agreement to well within a percent, and particle positions within a few kpc/ $h$ .

## V. SUMMARY AND OUTLOOK

In this paper we develop and discuss the techniques for relativistic  $N$ -body simulations in the weak field limit, keeping gravitational perturbations to first order, their spatial gradients to second order, and their second spatial derivatives to all orders. This corresponds to keeping velocities to second order and the density contrast (which alone is expected to become large) to all orders. In this way we are able to simulate structure formation in a general relativistic context, taking along the relativistic effects that can become relevant with current and future large cosmological surveys which will go out to redshifts of  $z \gtrsim 2$ . Relativistic simulations are also a natural approach to include relativistic fields like those needed for modified gravity simulations [47–51] or topological defects [1]. In addition, these simulations allow one to study whether backreaction effects become large and so to test the backreaction scenario.

The numerical challenges in implementing our formalism as an extension of a standard  $N$ -body code are manageable, but a full implementation still requires considerable effort. To test the scheme and to obtain initial results we have started with an effectively one-dimensional

implementation which allows one to treat plane-symmetric situations. Because plane symmetry does not admit vector and tensor perturbations, and precludes us from studying a realistic cosmological setup, we can only draw limited conclusions at this point. Our results show that, within this constrained setup, relativistic corrections to the traditional Newtonian treatment remain very small. We highlight three different types of corrections:

First, fixing the background FLRW solution by assuming an exactly pressureless equation of state for CDM, the scalar potential  $\Phi$  dynamically acquires a homogeneous mode. The homogeneous mode quantifies the backreaction and shows how the evolution of the averaged background slightly differs from the reference FLRW solution. With a relative amplitude of  $\sim 10^{-7}$  in the  $\Lambda$ CDM example, which is commensurate to the expected order of magnitude  $\sim v^2$ , it remains observationally irrelevant, but we want to make the point that its exact value can only be calculated consistently by taking into account all relevant terms at a given order. At order  $v^2$  there are, for instance, terms like  $\delta^{ij}\Phi_{,i}\Phi_{,j}$  which are important.

A second sign of relativistic corrections comes from considering the inhomogeneous component of  $\Phi - \Psi$ . As is well known, in linear perturbation theory  $\Phi - \Psi$  is sourced by anisotropic stress, which vanishes for a CDM source at linear order. It is therefore generated only at the nonlinear level (e.g. [52]). However, as explained in [26], it can be accurately estimated from Newtonian quantities. A comparison of our numerical results with this estimate is an excellent test for our algorithms. We demonstrate that the numerical scheme is able to give highly accurate results for this second order quantity, down to the truncation error which is introduced by discretization.

Finally, as a third way to quantify the difference between relativistic and purely Newtonian simulations, we look at the pairwise phase space correlation of individual particles between both simulation types when initialized on the same linear solution. We find that relativistic effects on the phase space trajectory of particles remain completely tolerable. In fact, the coordinates of individual  $N$ -body particles remain correlated to within a few kpc/ $h$  (comoving), and their velocities to within 1%.

All these observations have to be considered under the premise that our plane-symmetric setups are limited to scalar perturbations. However, recent quantitative analyses strongly suggest [53] that the inclusion of vector modes will also only have a small effect on the  $N$ -body dynamics, although there may be some potential for observing  $B_i$  through its effect on photon propagation. The same holds true for the tensor perturbations. A detailed quantitative comparison with three-dimensional Newtonian  $N$ -body simulations is in preparation. There we shall also calculate the induced vector and tensor perturbation spectra.

While observing relativistic effects within the context of  $\Lambda$ CDM standard cosmology will be challenging, we

should keep in mind that relativistic simulations of structure formation have a great potential in testing possible extensions to the standard model. For instance, cosmic neutrinos or a warm component of dark matter may constitute a semirelativistic source which is relevant during the process of structure formation. In the sector of dark energy it is also very important to be able to test various alternatives to a cosmological constant, and again it seems most promising to use large scale structure as a probe. Once the numerical scheme for general relativistic simulations is fully implemented, the challenge may lie in the modeling and evolution of the stress-energy tensor of the additional sources one wants to consider.

## ACKNOWLEDGMENTS

It is a pleasure to thank Chris Clarkson and Roy Maartens for interesting comments. J. A. acknowledges funding from the German Research Foundation (DFG) through the research fellowship AD 439/1-1. This work is supported by the Swiss National Science Foundation.

## APPENDIX A: LATTICE EQUATIONS

In this Appendix, we explicitly present the finite-difference operations which define the various algorithms presented in this paper. We assume that the code represents continuous fields (like, e.g., the metric) on a structured mesh of rank three, which can basically be identified with a comoving coordinate grid covering a spacelike hypersurface. We make use of the convenient notation  $f_{\mathbf{i},\mathbf{j},\mathbf{k}}^{\mathbf{n}} \doteq f(\tau_{\mathbf{n}}, x_{\mathbf{i},\mathbf{j},\mathbf{k}}^i)$ , where  $\mathbf{n}$  is a discrete index labeling the time steps, while  $\mathbf{i}, \mathbf{j}, \mathbf{k}$  are discrete indices labeling the grid points of the mesh. In some cases, a quantity may be defined with a fractional index whose meaning should be clear from the context. The grid spacing is given in units of  $dx^1, dx^2, dx^3$ , and the size of a time step is denoted as  $d\tau$ .

The evolution of dark matter will be given by the notion of test particles which move on timelike geodesics. Their coordinates  $x^i$  and velocities  $v^i = dx^i/d\tau$  are stored in a list and can take continuous values. Like in a standard particle-to-mesh  $N$ -body framework, the code therefore has to provide appropriate projection and interpolation operators in order to connect between grid-based and particle-based information. If dark matter is represented in a different way, or if one wants to include baryons or other types of interacting matter, it should still be more or less straightforward to implement the correct gravitational acceleration. We leave it as an exercise to the reader to figure out the appropriate prescription for their favorite hydrodynamical scheme.

### 1. ADI scheme

The alternate-direction-implicit (ADI) update for  $\Phi$  is carried out by splitting the operation into three steps, one

step for each spatial dimension. The idea is that each step amounts to only solving a linear tridiagonal system, which can be done very efficiently using the Thomas algorithm. There is no unique way of performing the split. We simply follow [44] and add the nonlinear terms in the most straightforward fashion. There may be better splitting

procedures, and it may be worthwhile to investigate in this direction. With three spatial dimensions, the update makes use of two intermediate solutions,  $\Phi^{n+\frac{1}{3}}$  and  $\Phi^{n+\frac{2}{3}}$ . These should not be interpreted as solutions at fractional time steps, but rather as auxiliary surrogates for  $\Phi^{n+1}$ . They obey following finite difference equations:

$$(1 + 4\Phi_{i,j,k}^n) \left( \frac{\Phi_{i-1,j,k}^{n+\frac{1}{3}} + \Phi_{i+1,j,k}^{n+\frac{1}{3}} - 2\Phi_{i,j,k}^{n+\frac{1}{3}}}{(dx^1)^2} + \frac{\Phi_{i,j-1,k}^n + \Phi_{i,j+1,k}^n - 2\Phi_{i,j,k}^n}{(dx^2)^2} + \frac{\Phi_{i,j,k-1}^n + \Phi_{i,j,k+1}^n - 2\Phi_{i,j,k}^n}{(dx^3)^2} \right) - 3\mathcal{H} \frac{\Phi_{i,j,k}^{n+\frac{1}{3}} - \Phi_{i,j,k}^n}{d\tau} - 3\mathcal{H}^2 \Psi_{i,j,k}^n + \frac{3}{2} \left( \frac{(\Phi_{i+1,j,k}^n - \Phi_{i-1,j,k}^n)^2}{4(dx^1)^2} + \frac{(\Phi_{i,j+1,k}^n - \Phi_{i,j-1,k}^n)^2}{4(dx^2)^2} + \frac{(\Phi_{i,j,k+1}^n - \Phi_{i,j,k-1}^n)^2}{4(dx^3)^2} \right) = 4\pi G a^2 \bar{\rho} \left[ \delta_{i,j,k}^n + 3\Phi_{i,j,k}^n (1 + \delta_{i,j,k}^n) + \frac{1}{2} (1 + \delta_{i,j,k}^{n+\frac{1}{2}}) \langle v^2 \rangle_{i,j,k}^{n+\frac{1}{2}} \right], \quad (\text{A1a})$$

$$(1 + 4\Phi_{i,j,k}^n) \frac{\Phi_{i,j-1,k}^{n+\frac{2}{3}} + \Phi_{i,j+1,k}^{n+\frac{2}{3}} - 2\Phi_{i,j,k}^{n+\frac{2}{3}}}{(dx^2)^2} = (1 + 4\Phi_{i,j,k}^n) \frac{\Phi_{i,j-1,k}^n + \Phi_{i,j+1,k}^n - 2\Phi_{i,j,k}^n}{(dx^2)^2} + 3\mathcal{H} \frac{\Phi_{i,j,k}^{n+\frac{2}{3}} - \Phi_{i,j,k}^{n+\frac{1}{3}}}{d\tau}, \quad (\text{A1b})$$

$$(1 + 4\Phi_{i,j,k}^n) \frac{\Phi_{i,j,k-1}^{n+1} + \Phi_{i,j,k+1}^{n+1} - 2\Phi_{i,j,k}^{n+1}}{(dx^3)^2} = (1 + 4\Phi_{i,j,k}^n) \frac{\Phi_{i,j,k-1}^n + \Phi_{i,j,k+1}^n - 2\Phi_{i,j,k}^n}{(dx^3)^2} + 3\mathcal{H} \frac{\Phi_{i,j,k}^{n+1} - \Phi_{i,j,k}^{n+\frac{2}{3}}}{d\tau}. \quad (\text{A1c})$$

Indeed, each equation is a linear tridiagonal problem. The stability of the scheme for a linear parabolic operator has been proven in [44]. This property can in principle be lost when nonlinear terms are present in the equation. However, we expect that in our case the nonlinearities remain sufficiently subdominant that this is not an issue.

Note that in the plane symmetric setup, the last two equations become trivial and simply imply  $\Phi^{n+\frac{1}{3}} = \Phi^{n+\frac{2}{3}} = \Phi^{n+1}$ , i.e. the auxiliary solutions are redundant.

## 2. Multigrid

In order to solve Eq. (12), we follow [43] and use a nonlinear multigrid scheme (“FAS algorithm”) coupled to a Newton-Gauß-Seidel relaxation method. The key equation is (20.6.43) of [43], identifying  $u_i$  with our sought-after  $\Psi_{i,j,k}^n$  and using the discretized operator

$$\begin{aligned} \mathcal{L}(\Psi_{i,j,k}^n) &\doteq (1 + 2\Phi_{i,j,k}^n - 2\Psi_{i,j,k}^n) \left( \frac{\Psi_{i-1,j,k}^n + \Psi_{i+1,j,k}^n - 2\Psi_{i,j,k}^n}{(dx^1)^2} + \dots \right) \\ &\quad - \frac{(\Psi_{i+1,j,k}^n - \Psi_{i-1,j,k}^n)(\Phi_{i+1,j,k}^n - \Phi_{i-1,j,k}^n + \Psi_{i+1,j,k}^n - \Psi_{i-1,j,k}^n)}{4(dx^1)^2} - \dots \\ &\quad + \frac{1}{\mathcal{H}} \left[ \left( 1 + 4\Phi_{i,j,k}^n \right) \left( \frac{\Phi_{i-1,j,k}^n - \Phi_{i-1,j,k}^{n-1} + \Phi_{i+1,j,k}^n - \Phi_{i+1,j,k}^{n-1} - 2\Phi_{i,j,k}^n + 2\Phi_{i,j,k}^{n-1}}{d\tau(dx^1)^2} + \dots \right) \right. \\ &\quad + 4 \frac{\Phi_{i,j,k}^n - \Phi_{i,j,k}^{n-1}}{d\tau} \left( \frac{\Phi_{i-1,j,k}^n + \Phi_{i+1,j,k}^n - 2\Phi_{i,j,k}^n}{(dx^1)^2} + \dots \right) \\ &\quad \left. + 3 \frac{(\Phi_{i+1,j,k}^n - \Phi_{i+1,j,k}^{n-1} - \Phi_{i-1,j,k}^n + \Phi_{i-1,j,k}^{n-1})(\Phi_{i+1,j,k}^n - \Phi_{i-1,j,k}^n)}{4d\tau(dx^1)^2} + \dots \right] \\ &\quad + \frac{4\pi G a^2 \bar{\rho}}{\mathcal{H}} \left[ \left( 1 + 3\Phi_{i,j,k}^n \right) \left( \frac{((1 + \delta)\langle \gamma v^1 \rangle)_{i+\frac{1}{2},j,k}^{n-\frac{1}{2}} - ((1 + \delta)\langle \gamma v^1 \rangle)_{i-\frac{1}{2},j,k}^{n-\frac{1}{2}}}{dx^1} + \dots \right) \right. \\ &\quad \left. + \frac{((1 + \delta)\langle \gamma v^1 \rangle)_{i+\frac{1}{2},j,k}^{n-\frac{1}{2}} + ((1 + \delta)\langle \gamma v^1 \rangle)_{i-\frac{1}{2},j,k}^{n-\frac{1}{2}}}{2} \times \frac{\Psi_{i+1,j,k}^n - \Psi_{i-1,j,k}^n}{2dx^1} + \dots - 3\delta_{i,j,k}^n \frac{\Phi_{i,j,k}^n - \Phi_{i,j,k}^{n-1}}{d\tau} \right]. \quad (\text{A2}) \end{aligned}$$

Here, the ellipses indicate that the previous term has to be written also for the other two directions  $x^2$  and  $x^3$  accordingly. Note that our operator  $\mathcal{L}$  is only accurate to first order in time although one could easily modify it such that it would be accurate to second order. However, since the ADI algorithm used for the evolution of  $\Phi$  is a first order scheme, the implementation of a second order scheme for  $\Psi$  would probably not increase the overall accuracy.

We perform the relaxation sweep in the ‘‘checkerboard’’ fashion, such that updated values on neighboring sites are already available when updating site  $(\mathbf{i}, \mathbf{j}, \mathbf{k})$ . We also store the approximate solution for all multigrid levels between time steps, such that the previous solution can be used as an initial guess in the next step. Since the potential  $\Psi$  varies slowly in time, this initial guess is already very close to the final solution. Tracking the solution in such a way, we found that the multigrid algorithm generally needs no more than a single V-cycle to meet the convergence criterion again after one time step. Note that the additional memory to store the coarse-grid approximations, in 3D, is bounded by  $1/7 \simeq 15\%$  of the memory consumed by the full resolution.

### 3. Loop structure

As usual, we perform the particle updates in a leapfrog fashion, i.e. we associate particle positions and acceleration to integer time steps, while velocities are associated to half-integer time steps. A complete loop of one time step of our algorithm can be sketched as follows:

- (i) update velocities:

$$(\mathbf{v}^i)^{n+\frac{1}{2}} = \frac{(\mathbf{v}^i)^{n-\frac{1}{2}}(1 - \frac{d\tau}{2} \mathcal{H}) - d\tau \nabla \Psi^n}{1 + \frac{d\tau}{2} \mathcal{H}} \quad (\text{A3})$$

- (ii) update positions by half a step:

$$(x^i)^{n+\frac{1}{2}} = (x^i)^n + \frac{d\tau}{2} (\mathbf{v}^i)^{n+\frac{1}{2}} \quad (\text{A4})$$

- (iii) do particle-to-mesh projection for  $((1 + \delta) \times \langle \gamma \mathbf{v}^i \rangle)^{n+\frac{1}{2}}$  (face centered, i.e. onto a mesh shifted by half a grid unit in direction  $x^i$ ) and  $(1 + \delta^{n+\frac{1}{2}}) \times \langle \mathbf{v}^2 \rangle^{n+\frac{1}{2}}$  (cell centered)

- (iv) update  $\Phi^n \rightarrow \Phi^{n+1}$

- (v) update positions by half a step:

$$(x^i)^{n+1} = (x^i)^{n+\frac{1}{2}} + \frac{d\tau}{2} (\mathbf{v}^i)^{n+\frac{1}{2}} \quad (\text{A5})$$

- (vi) do particle-to-mesh projection for  $\delta^{n+1}$

- (vii) compute  $\Psi^{n+1}$

- (viii)  $\mathbf{n} + + \dots$

The gradient of  $\Psi$ , and other metric terms, have to be interpolated to the particle positions when updating the velocities, as will be specified in the next subsection. The loop shown here only includes the scalar degrees of freedom

and is sufficient for the plane-symmetric case. When vector modes are taken into account, the update of the particle velocities has to be modified accordingly, and the vector component of the metric has to be computed at an appropriate instance within the loop. Finally, if desired, one can also insert the evolution step of the tensor component.

### 4. Particle-to-mesh projection and force interpolation

In order to establish the connection between grid-based and particle-based information, we make use of some standard approaches which are detailed in [54]. There, a systematic hierarchy of prescriptions which assign particle properties to grid points is developed, explicitly discussing nearest-grid-point, cloud-in-cell (CIC), and triangular-shaped-particle (TSP) as the first three members of this hierarchy. Generally speaking, one can trade a reduction of discretization errors for a more complicated assignment scheme.

As a guiding principle, since we are explicitly using conservation of stress energy to arrive at Eq. (12), we aim for an assignment scheme which guarantees to satisfy the discrete version of the continuity equation,

$$[a^3 \rho]' + a^3 [\rho u^i]_{,i} = 0, \quad (\text{A6})$$

where the divergence of the momentum density is discretized precisely in the same way as in Eq. (A2).

Choosing to construct  $a^3 \rho$  with the TSP assignment scheme, one can analytically check that the above equation holds identically if we construct  $a^3 \rho u^i$  using CIC assignment in direction  $x^i$  (on the face-centered grid), and TSP assignment in the remaining directions. We trivially add the  $\mathbf{v}^2$  corrections by multiplying the result for each particle by  $1 + \mathbf{v}^2/2$ , which accounts for the kinetic energy density or Lorentz factor, respectively.

The interpolation of the grid-based field information to the particle positions must be done in such a way that the resulting force does not include a relevant self-force. According to [54], it is generally sufficient if the force interpolation scheme is at most of the same polynomial order as the particle-to-mesh assignment scheme, at least when all equations are linear. We do not expect that nonlinearities introduce an instability in our case, and so far our numerical simulations have shown no indication for such an instability. In practice, we used CIC force interpolation.

## APPENDIX B: INITIAL CONDITIONS FOR NEWTONIAN AND RELATIVISTIC SIMULATIONS

The smallness of perturbations in the early Universe allows us to pose the initial conditions at a time when perturbation theory is valid. Traditionally, the well-known solutions of linear perturbation theory have been used for

this purpose, although people have also started to consider results from second order perturbation theory [55]. We shall discuss only the former approach, although ultimately, implementing the latter one is certainly desirable as it would guarantee that all second order terms within our framework are accurate. However, for the purpose of this work, we simply always chose the initial redshift high enough that second order terms can safely be neglected, giving our simulation enough time to evolve to the nonlinear solution on its own.

As shown by Bardeen [56], linear cosmological perturbations can be characterized completely in terms of gauge-invariant quantities. Once the linear solutions for these quantities have been determined, it is just a matter of relating gauge-dependent quantities to these solutions in order to obtain the linear solutions in any gauge. In the longitudinal gauge which we use in our relativistic framework, these relations are given by

$$\Psi = \Psi Q^{(S)}, \quad (\text{B1a})$$

$$\Phi = \Phi Q^{(S)}, \quad (\text{B1b})$$

$$B_i = \sigma^{(V)} Q_i^{(V)}, \quad (\text{B1c})$$

$$h_{ij} = 2H^{(T)} Q_{ij}^{(T)}, \quad (\text{B1d})$$

$$u^i = V Q^{(S)i} + V^{(V)} Q^{(V)i}, \quad (\text{B1e})$$

$$\delta + 3\Phi = D_g Q^{(S)}, \quad (\text{B1f})$$

where the functions  $Q^{(S)}$ ,  $Q_i^{(V)}$ ,  $Q_{ij}^{(T)}$  denote the scalar, vector, and tensor Fourier modes, respectively, and the amplitudes are given in the notation of [57]. In particular, we use the same notation for  $\Phi$ ,  $\Psi$  and its Fourier transform.  $V$  and  $V^{(V)}$  denote the gauge-invariant amplitudes of the scalar (curl-free) and vector (divergence-free) parts of a Helmholtz decomposition of the velocity field, respectively, and  $D_g$  is a possible gauge-invariant amplitude of the density perturbation. The left-hand side of the last line is obtained by truncating our expression for the energy density, Eq. (7), at linear order. At this level, the anisotropic stress of nonrelativistic matter is negligible, as is its effective pressure.

It is usually assumed that vector modes are not significantly excited in the early Universe or have had time to decay until the onset of matter domination. One can then consistently set  $\sigma^{(V)} = V^{(V)} = 0$  during linear evolution, which sets  $B_i = 0$  and implies that  $u^i$  is given by the gradient of a scalar function.

At linear order, scalar, vector, and tensor equations decouple and can be analyzed separately. Furthermore, in Fourier space, Einstein's equations reduce to a system of ordinary differential equations for the gauge-invariant amplitudes in each sector. In the scalar sector, this system is second order in time, giving two independent solutions. For the matter dominated era, these can be found analytically,

$$\Phi = \Psi = c_1 + c_2 \tau^{-5}, \quad (\text{B2a})$$

$$V = \frac{k}{3} c_1 \tau - \frac{k}{2} c_2 \tau^{-4}, \quad (\text{B2b})$$

$$D_g = -\frac{k^2}{6} \left(1 + 3 \frac{\mathcal{H}^2}{k^2}\right) c_1 \tau^2 - \frac{k^2}{6} \left(1 - \frac{9\mathcal{H}^2}{2k^2}\right) c_2 \tau^{-3}, \quad (\text{B2c})$$

where  $c_1$  and  $c_2$  are the two constants of integration. The solution proportional to  $c_2$  decays rapidly and is usually discarded. One then arrives at the well-known result that the gauge-invariant Bardeen potentials  $\Psi$  and  $\Phi$  are constant (and equal) during matter domination. The linear solution for the other gauge-invariant quantities is uniquely determined once these potentials are specified.

The vector equations are only first order in time, and the solution for the ‘‘frame-dragging potential’’ reads  $\sigma^{(V)} \propto \tau^{-4}$  in the matter dominated era. Since this solution decays,  $B_i = 0$  as initial condition remains a reasonable choice.

The tensor equations are again second order in time. As already mentioned in Sec. III, the two independent free solutions for  $H^{(T)}$  are given by  $(k\tau)^{-1} j_1(k\tau)$  and  $(k\tau)^{-1} y_1(k\tau)$ , with  $j_1$  and  $y_1$  spherical Bessel functions. Both solutions oscillate and decay inside the horizon,  $k\tau \gg 1$ . However, outside the horizon, only the latter one decays, while the former one remains approximately constant. Its amplitude is determined by early Universe physics. Usually, one assumes that these superhorizon modes are generated during inflation, at the time when they exit the horizon. They can be constrained, e.g., by observations of the cosmic microwave background. Thus far, only upper limits have been obtained, and observations are therefore compatible with the choice  $h_{ij} = 0$  as initial condition on all scales.

Our strategy to generate initial data is then the following. First, we specify the initial potentials  $\Phi = \Psi$ . Choosing the constant solution, we also have  $\Phi' = 0$ . Next, we have to generate initial data for the particle list. Starting from a uniform particle distribution, the initial positions of the particles can be assigned by an infinitesimal displacement, given by the gradient of a scalar function,  $\delta x^i = \delta^{ij} \zeta_{,j}$ . The resulting bare mass density contrast will be  $\delta = -\Delta \zeta$ . The scalar function  $\zeta$  is then uniquely (up to an irrelevant homogeneous piece) determined by the linearized version of Eq. (8),

$$\Delta \Phi - 3\mathcal{H}^2 \Psi = 4\pi G a^2 \bar{\rho} (-\Delta \zeta + 3\Phi). \quad (\text{B3})$$

This linear relation can be solved algebraically with the Fourier method. Equivalently, one could determine  $\zeta$  using the relations (B1) and the linear solutions (B2).

Assuming a negligible initial velocity dispersion, the initial peculiar velocities of the particles can be worked out from Eqs. (B1) and (B2) as well. Ignoring again the decaying solution, one finds

$$\frac{dx^i}{d\tau} = -\frac{2}{3\mathcal{H}} \delta^{ij} \Psi_{,j}. \quad (\text{B4})$$

In fact, Eqs. (B3) and (B4) can simply be regarded as the Zel'dovich approximation in longitudinal gauge. It is worth noting the important difference to the corresponding approximation which is used to generate initial data for Newtonian  $N$ -body simulations. In Newtonian gravity, the concept of a horizon is absent, and one wants Eq. (2) to hold on all scales. It is therefore reasonable to identify the initial density perturbation  $\delta$  with another gauge-invariant measure thereof, namely the density perturbation in comoving gauge, which is denoted by  $D$  in [57] and is related to the gauge-invariant potential  $\Phi$  precisely by Eq. (2). The Newtonian potential  $\psi_N$  is then again identified with  $\Phi = \Psi$ . These identifications can be done consistently because there is an exact correspondence between the Newtonian and relativistic solutions (taken in an appropriate gauge and assuming a pressureless equation of state) at the level of scalar linear perturbations. This correspondence breaks down at the nonlinear level (or if the pressureless assumption is not valid), and the Newtonian and relativistic solutions live in completely different worlds. Most importantly, there is no particular gauge where Newtonian quantities can be identified with relativistic ones. All one can hope is that there is an approximate correspondence which

is reasonable for practical purposes, and this is the idea behind the dictionary which was proposed in [26].

Owing to the gauge dependence of the density contrast  $\delta$ , the initial particle configuration for the same linear solution (B2) is *different* for a relativistic simulation compared to a Newtonian one. In particular, the Newtonian Zel'dovich approximation simply has  $\zeta = -2\psi_N/3\mathcal{H}^2$ , which corresponds to the relativistic expression in comoving gauge. In the longitudinal gauge employed in our framework,  $\zeta$  is given by Eq. (B3). Evidently, on very long wavelengths where  $k \ll \mathcal{H}$ , we have that  $\Delta\zeta \propto \Phi$  and thus  $\zeta$  can become large. This is, however, not a practical problem as the density contrast  $\delta$  (and therefore the perturbation of the particle number density) is of order  $\Phi$  by construction and thus small. The long wavelength part of  $\zeta_j$  is just a constant time-independent shift acting on a “fictitious” regular particle configuration that has no physical significance. In particular, this configuration is never physically realized, even if one follows the particle trajectories backwards in time. Note also that on super-horizon scales, where perturbations are always linear, one can always translate between different gauges by employing a linear gauge transformation.

- 
- [1] M. Obradovic, M. Kunz, M. Hindmarsh, and I. T. Iliev, *Phys. Rev. D* **86**, 064018 (2012).
  - [2] P. Brax, C. Burrage, and A.-C. Davis, *J. Cosmol. Astropart. Phys.* **10** (2012) 016.
  - [3] J. Magueijo, A. Albrecht, P. Ferreira, and D. Coulson, *Phys. Rev. D* **54**, 3727 (1996).
  - [4] R. Durrer and M. Kunz, *Phys. Rev. D* **57**, R3199 (1998).
  - [5] I. D. Saltas and M. Kunz, *Phys. Rev. D* **83**, 064042 (2011).
  - [6] C. Bonvin, R. Durrer, and M. A. Gasparini, *Phys. Rev. D* **73**, 023523 (2006).
  - [7] C. Bonvin and R. Durrer, *Phys. Rev. D* **84**, 063505 (2011).
  - [8] A. Challinor and A. Lewis, *Phys. Rev. D* **84**, 043516 (2011).
  - [9] D. Bertacca, R. Maartens, A. Raccanelli, and C. Clarkson, *J. Cosmol. Astropart. Phys.* **10** (2012) 025.
  - [10] O. Umeh, C. Clarkson, and R. Maartens, [arXiv:1207.2109](https://arxiv.org/abs/1207.2109).
  - [11] I. Ben-Dayan, G. Marozzi, F. Nugier, and G. Veneziano, *J. Cosmol. Astropart. Phys.* **11** (2012) 045.
  - [12] C. Bonvin, R. Durrer, and M. Kunz, *Phys. Rev. Lett.* **96**, 191302 (2006).
  - [13] A. Abate and O. Lahav, *Mon. Not. R. Astron. Soc.* **389**, L47 (2008).
  - [14] W. Valkenburg, M. Kunz, and V. Marra, [arXiv:1302.6588](https://arxiv.org/abs/1302.6588).
  - [15] I. Ben-Dayan, M. Gasperini, G. Marozzi, F. Nugier, and G. Veneziano, *J. Cosmol. Astropart. Phys.* **06** (2013) 002.
  - [16] V. Marra, L. Amendola, I. Sawicki, and W. Valkenburg, *Phys. Rev. Lett.* **110**, 241305 (2013).
  - [17] P. Fleury, H. Dupuy, and J.-P. Uzan, *Phys. Rev. Lett.* **111**, 091302 (2013).
  - [18] S. Räsänen, *J. Cosmol. Astropart. Phys.* **11** (2006) 003.
  - [19] T. Buchert, *Gen. Relativ. Gravit.* **40**, 467 (2008).
  - [20] S. Räsänen, *Classical Quantum Gravity* **28**, 164008 (2011).
  - [21] C. Clarkson, G. Ellis, J. Larena, and O. Umeh, *Rep. Prog. Phys.* **74**, 112901 (2011).
  - [22] T. Buchert and S. Räsänen, *Annu. Rev. Nucl. Part. Sci.* **62**, 57 (2012).
  - [23] S. Räsänen, *Phys. Rev. D* **81**, 103512 (2010).
  - [24] M. Shibata and K. Taniguchi, *Living Rev. Relativity* **14**, 6 (2011).
  - [25] S. R. Green and R. M. Wald, *Phys. Rev. D* **83**, 084020 (2011).
  - [26] S. R. Green and R. M. Wald, *Phys. Rev. D* **85**, 063512 (2012).
  - [27] R. Rampf and G. Rigopoulos, *Phys. Rev. D* **87**, 123525 (2013).
  - [28] G. Rigopoulos and W. Valkenburg, [arXiv:1308.0057](https://arxiv.org/abs/1308.0057).
  - [29] J. Adamek, E. Di Dio, R. Durrer, and M. Kunz (unpublished).
  - [30] R. Brustein, M. Gasperini, M. Giovannini, V. F. Mukhanov, and G. Veneziano, *Phys. Rev. D* **51**, 6744 (1995).
  - [31] C. Cartier, R. Durrer, and E. J. Copeland, *Phys. Rev. D* **67**, 103517 (2003).
  - [32] S. J. Turnbull, M. J. Hudson, H. A. Feldman, M. Hicken, R. P. Kirshner, and R. Watkins, *Mon. Not. R. Astron. Soc.* **420**, 447 (2012).
  - [33] G. Efstathiou, M. Davis, C. Frenk, and S. D. White, *Astrophys. J. Suppl. Ser.* **57**, 241 (1985).
  - [34] S. J. Aarseth, *Gravitational N-body Simulations: Tools and Algorithms* (Cambridge University Press, Cambridge, England, 2003).

- [35] V. Springel, S.D. White, A. Jenkins, C.S. Frenk, N. Yoshida *et al.*, *Nature (London)* **435**, 629 (2005).
- [36] V. Springel, J. Wang, M. Vogelsberger, A. Ludlow, A. Jenkins, A. Helmi, J. F. Navarro, C. S. Frenk, and S. D. M. White, *Mon. Not. R. Astron. Soc.* **391**, 1685 (2008).
- [37] T. Matsubara, *Astrophys. J. Lett.* **537**, L77 (2000).
- [38] N. E. Chisari and M. Zaldarriaga, *Phys. Rev. D* **83**, 123505 (2011).
- [39] J. Colberg *et al.* (VIRGO Collaboration), *Mon. Not. R. Astron. Soc.* **319**, 209 (2002).
- [40] A. Evrard *et al.* (VIRGO Collaboration), *Astrophys. J.* **573**, 7 (2002).
- [41] S. Gottlober, G. Yepes, A. Khalatyan, R. Sevilla, and V. Turchaninov, *AIP Conf. Proc.* **878**, 3 (2006).
- [42] C. Park, J. Kim, and J.R. Gott III, *Astrophys. J.* **633**, 1 (2005).
- [43] W.H. Press, S. A. Teukolsky, W. T. Vetterling, and B.P. Flannery, *Numerical Recipes* (Cambridge University Press, Cambridge, England, 2007), Chap. 20, 3rd ed.
- [44] J. Douglas and H. H. Rachford, *Trans. Am. Math. Soc.* **82**, 421 (1956).
- [45] J. Douglas, *Numer. Math.* **4**, 41 (1962).
- [46] N. Mattor, T.J. Williams, and D.W. Hewett, *Parallel Comput.* **21**, 1769 (1995).
- [47] K. Chan and R. Scoccimarro, *Phys. Rev. D* **80**, 104005 (2009).
- [48] B. Li, G.-B. Zhao, R. Teyssier, and K. Koyama, *J. Cosmol. Astropart. Phys.* **01** (2012) 051.
- [49] J. Lee, G.-B. Zhao, B. Li, and K. Koyama, *Astrophys. J.* **763**, 28 (2013).
- [50] P. Brax, A.-C. Davis, B. Li, H. A. Winther, and G.-B. Zhao, *J. Cosmol. Astropart. Phys.* **04** (2013) 029.
- [51] E. Puchwein, M. Baldi, and V. Springel, [arXiv:1305.2418](https://arxiv.org/abs/1305.2418).
- [52] G. Ballesteros, L. Hollenstein, R. K. Jain, and M. Kunz, *J. Cosmol. Astropart. Phys.* **05** (2012) 038.
- [53] M. Bruni, D. B. Thomas, and D. Wands, [arXiv:1306.1562](https://arxiv.org/abs/1306.1562).
- [54] R. W. Hockney and J. W. Eastwood, *Computer Simulation Using Particles* (Institute of Physics Publishers, Bristol, England, 1999).
- [55] M. Crocce, S. Pueblas, and R. Scoccimarro, *Mon. Not. R. Astron. Soc.* **373**, 369 (2006).
- [56] J. M. Bardeen, *Phys. Rev. D* **22**, 1882 (1980).
- [57] R. Durrer, *The Cosmic Microwave Background* (Cambridge University Press, Cambridge, England, 2008).